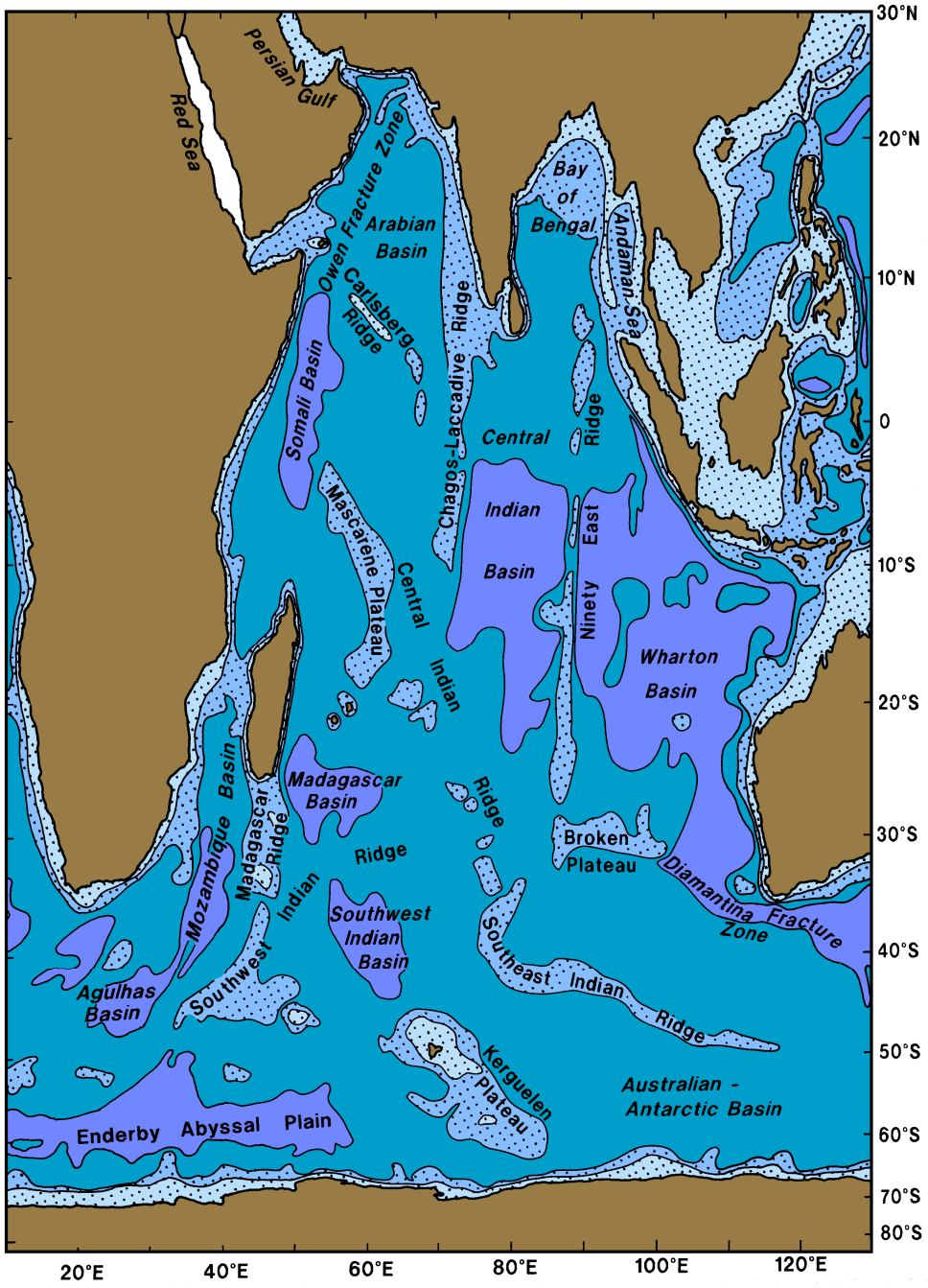

Fig. 11.1. Topography of the Indian Ocean. The 1000, 3000, and 5000 m isobaths are shown, and regions less than 3000 m deep are shaded. South of Australia the Indian Ocean extends to Tasmania (146° 55'E). See Figure 8.3 for the topography east of 125°E.

year. The wind also carries dry air, and the Winter Monsoon season is the dry season for most of southern Asia.

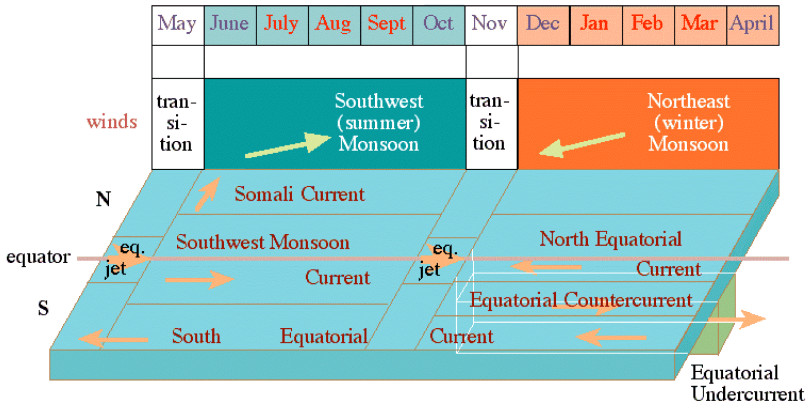

Fig. 11.2. A summary of the monsoon system in the Indian Ocean. The top part indicates the wind cycle, the lower part shows the major currents that develop in response to the wind.

The situation in the southern hemisphere is dominated by the pressure gradient between the tropical low and the subtropical high pressure belts. The axis of low pressure in the tropics is near 10°S, while the subtropical high pressure belt is dominated by an air pressure maximum 1000 km north of the Kerguelen Islands. The resulting Southeast Trades are rather uniform and somewhat stronger than in the Pacific Ocean. As in the other oceans the Trades are southerly along the eastern coast, but over Australia's Northwest Shelf winds become south-westerly, skirting the heat low over that continent. This brings summer rain to northern Australia. Rain also occurs throughout the Doldrums, with maximum rainfall in the Indonesian region.

The *Southwest* or *Summer Monsoon* determines the climate of the northern Indian Ocean during the northern hemisphere summer (June - September). A deep heat low develops over northern Arabia and Pakistan. The Australian heat low of the southern summer is replaced by a centre of high pressure, while the atmospheric high north of the Kerguelen Islands is shifted westward towards southern Africa. Whereas during the winter monsoon season the north-south pressure gradient from Arabia to Madagascar barely exceeds 6 hPa, there is now a gradient of 22 hPa acting in the opposite direction. As a result the winds in the northern Indian Ocean reverse completely and are no longer like the Trades anywhere. A wind jet, believed to be an atmospheric version of a western boundary current, develops along the high east African topography. Winds blow steadily at Beaufort 6 or more over the entire western Indian Ocean north of the equator. Further east along the equator the winds weaken, bringing moderate rainfall; but there is still a southerly component throughout the entire Indian Ocean everywhere north of 30°S. On the Northwest Shelf the wind blows directly offshore with moderate strength.

knowledge, the annual mean transports of the open-ocean currents are well predicted by the Sverdrup relation, and the transports of the East Madagascar, Mozambique, and Agulhas Currents follow quite accurately from mass continuity.

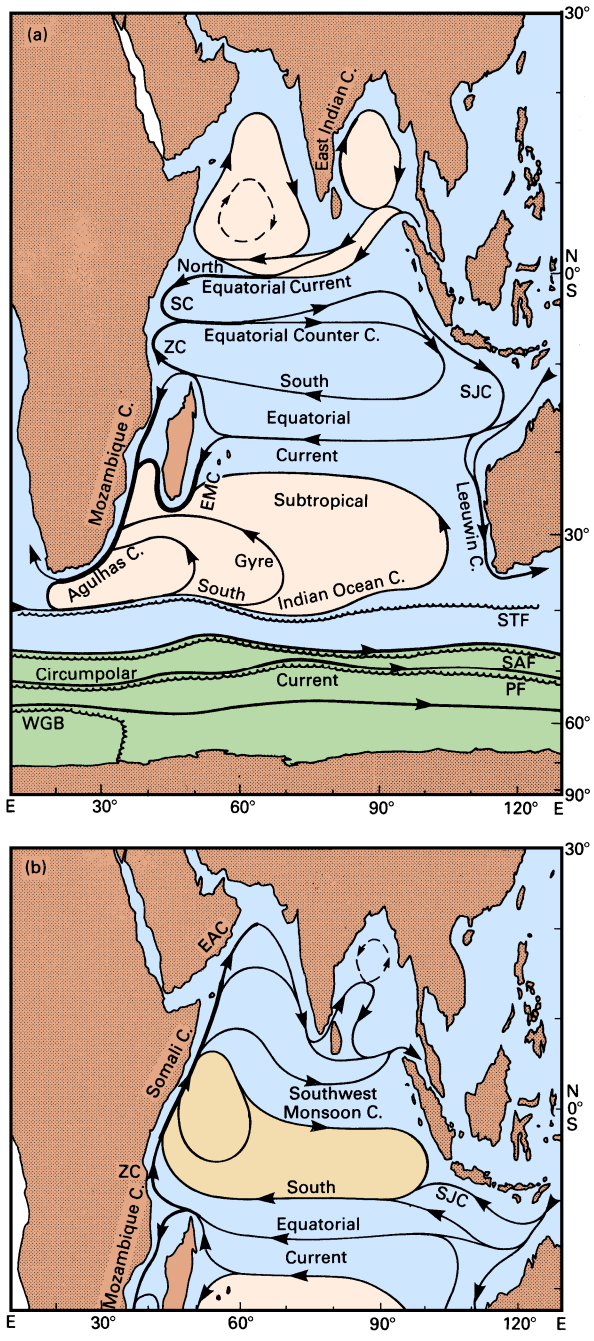

Fig. 11.3. Surface currents in the Indian Ocean.

top: late Northeast Monsoon season (March - April);

bottom: late Southwest Monsoon season (September - October; the circulation south of 20°S remains unchanged).

Abbreviations are used for the East Arabian (EAC), South Java (SJC), Zanzibar (ZC), East Madagascar (EMC), and Somali (SC) Currents. Other abbreviations denote fronts: STF: Subtropical Front, SAF: Subantarctic Front, PF: Antarctic Polar Front, WGB: Weddell Gyre Boundary.

The Indonesian throughflow from the Pacific Ocean enters the Indian Ocean during both seasons as a narrow band of low salinity water. It is embedded in generally westward flow and therefore apparently does not develop the strong lateral shear necessary to induce much instability. It continues westward, providing the core of maximum westward flow in the equatorial current system, and can be followed over the entire width of the Indian Ocean.

The subtropical gyre of the southern hemisphere is seen with two western boundary currents, one along eastern Madagascar and one along the coast of Mozambique. Whether both feed into the Agulhas Current - as indicated by the depth-integrated flow - or whether the East Madagascar Current feeds back into the gyre independently has been the subject of debate for some time and will be discussed in more detail later on. Here we only note the difference between the flow fields based on 1500 m and 2500 m levels of no motion (Figs 4.5 and 4.6) south of Madagascar; they indicate that the circulation near the end of the East Madagascar Current reaches deeper than 1500 m, not unlike the situation found in separation regions of other western boundary currents. The fact that deep flow is not restricted to the Agulhas Current but extends eastward away from Madagascar makes the estimation of transports in the gyre difficult and affects in particular our estimates for the South Equatorial Current.

The equatorial current system

Cutler and Swallow (1984) used the records of ship drifts collected by the British Meteorological Office from daily log book entries of merchant ships, to compile an atlas of surface currents. Currents in the Indian Ocean are stronger than in the Pacific or Atlantic Oceans during most of the year, which makes ship drift estimates reasonably reliable. Given the paucity of other information, this atlas is the best source of information on surface currents near the equator. Information on the subsurface structure became available with the long-term current meter moorings and time series of vertical current profiles taken during INDEX; unfortunately it is restricted to the region west of 62°E.

The evolution of surface currents through the seasons is shown in Figure 11.4. The *North Equatorial Current* is prominent in January and March when the Northeast Monsoon is fully established. It runs as a narrow current of about 0.3 m s^{-1} from Malacca Strait to southern Sri Lanka, where it bends southward and accelerates to reach 0.5 - 0.8 m s^{-1} between 2°S and 5°N in the region between 60°E and 75°E. The *South Equatorial Current* occupies the region south of 8°S with velocities rarely exceeding 0.3 m s^{-1}. Between these westward flows runs the *Equatorial Countercurrent* with 0.5 - 0.8 m s^{-1} in the west but getting weaker in the east; in January it does not reach beyond 70°E, being opposed in the east by weak westward flow.

The transition from Northeast to Southwest Monsoon (Figure 11.4c) is characterized by the intense *Indian Equatorial Jet* first described by Wyrtki (1973a). The long-term mean distributions derived from the ship drift data show it from early April until late June with velocities of 0.7 m s^{-1} or more. It is possible that in any particular year the jet appears within the three-month window April - June as a feature of shorter (one month) duration with higher peak velocities. The averaging employed with the ship drift data would spread it over the three months as a weaker feature. The jet is easily observed with drifting buoys since the current converges at the equator, keeping drifting objects trapped near its core. Away from the equator the current speed falls off to less than 0.2 m s^{-1} at 3°S or 3°N.

band along the equator it reaches its peak in November with velocities of 1.0 - 1.3 m s^{-1} and disappears in early January, when the annual cycle is repeated.

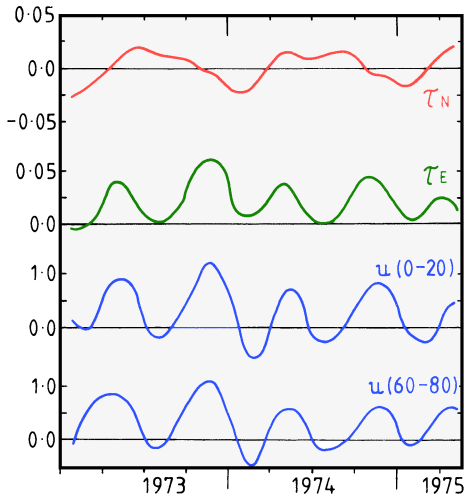

Fig. 11.5. Monthly mean winds and currents during 1973 - 1975 near the equator at 73°E: Meridional wind stress component τ_N (Pa), zonal wind stress component τ_E (Pa), and zonal velocities (m s^{-1}) averaged over 20 m for 0 - 20 m and 60 - 80 m depth. All directions indicate where currents and winds are going, north and east are positive. After McPhaden (1982).

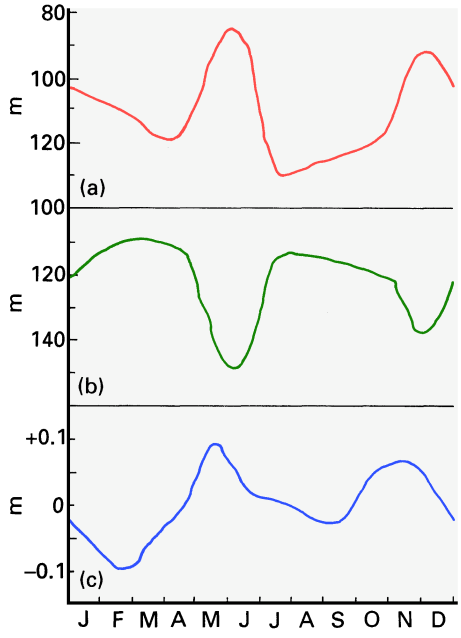

Fig. 11.6. Climatological mean monthly thermocline depth and sea level at the equator.

(a) Depth of 20°C isotherm off Africa,

(b) depth of 20°C isotherm off Sumatra,

(c) sea level at the west coast of Sumatra. After Wyrtki (1973a)

A remarkable feature of the equatorial current system is the dominance, within the annual monsoon cycle, of a semi-annual flow reversal in a narrow band along the equator. Figure 11.5 compares $2^1/_2$ years of wind data near the equator with average currents in two

much greater depths as well. During the Southwest Monsoon of 1976 mean flow at moorings in the area 52 - 58°E was westward with a northward component into the Somali basin at 500 m and 1500 m depth.

The oscillations of the undercurrent known from the Pacific and Atlantic Oceans occur in the Indian Ocean as well. At 200 m depth they were seen from August 1979 until January 1980 (in a record which covered the period March 1979 - June 1980). They were of 1300 km wavelength and 0.2 m s^{-1} meridional amplitude and shifted the undercurrent axis back and forth by about 150 km either side of the equator. Drifting buoy data for the period 1979 - 1982 indicate that at the peak of the Southwest Monsoon in August and September the oscillations reach into the surface layer with meridional flow amplitudes up to 0.8 m s^{-1}.

Circulation in the Arabian Sea and Bay of Bengal

Seasonal reversal of the currents dominates the two major subdivisions of the northern Indian Ocean as well, but the opposing flows occupy periods of very different length, and the transitions are less well defined than in the equatorial zone. Weak westward flow, an extension of the North Equatorial Current with velocities rarely exceeding 0.2 m s^{-1}, dominates in the Arabian Sea at the peak of the Northeast Monsoon season. Northwestward flow along the western Indian shelf begins as early as November (Figure 11.4f) and persists into January, with a width of some 400 km and a depth of about 200 m in the south (10°N), getting narrower and deeper as it flows along the continental slope. This current flows against the prevailing Northeast Monsoon and thus cannot be wind driven. The East Indian Winter Jet supplies fresh, low density water from the Bay of Bengal at this time, while on the north Indian coast cold continental winds result in cooling and convective overturn (Shetye *et al.*, 1991). The resulting gradient of steric height overwhelms the wind forcing. These dynamics are discussed in more detail with the Leeuwin Current below.

Westward flow prevails south of 15°N and west of 65°E until late April, while in the remaining area currents are less and less well defined and change gradually into the weak anticyclonic pattern of Figure 11.4b. The Somali Current responds quickly to the onset of the Southwest Monsoon in April; northward flow develops, strengthening the pattern in the west. By mid-May (Figure 11.4c) the *East Arabian Current* is fully established with velocities of 0.5 - 0.8 m s^{-1}. At the same time the anti-cyclonic pattern breaks up from the east where the flow joins the Equatorial Jet around southern India and Sri Lanka. Moderate eastward flow, an extension of the Somali and Southwest Monsoon Current dominates the region during the next 4 - 5 months. During its peak in June and July it reaches 0.3 m s^{-1} and more but weakens rapidly in October when the second occurrence of the Equatorial Jet concentrates most eastward transport in the equatorial zone and outflow from the Bay of Bengal begins to oppose eastward flow around Sri Lanka. By mid-November currents are again diffuse; south of 15°N they are weak but already westward. General westward flow is again established by early December.

A notable feature of the Arabian Sea circulation is the occurrence of strong coastal upwelling in the East Arabian Current. As in other coastal upwelling regions it owes its existence to an offshore transport direction in the Ekman layer (the Southwest Monsoon blowing parallel to the coast with the coast on its left). Positive curl(τ/f) over a 400 km wide strip along the coast adds to the upwelling through Ekman suction. From May to

variable again. The highest velocities (around 0.5 m s^{-1}) are found in the East Indian Current; flow along the eastern coast rarely exceeds 0.2 m s^{-1} but is often directed into the wind.

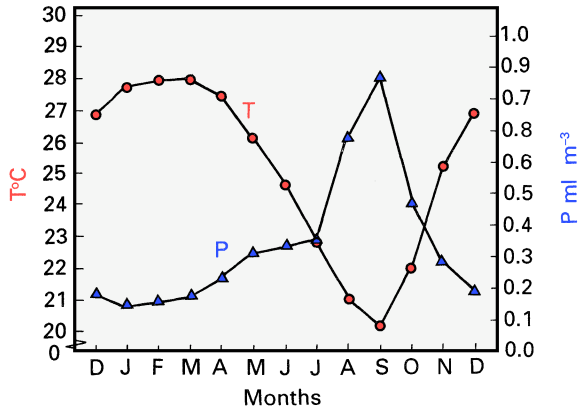

Fig. 11.9. Monthly mean temperature at 50 m depth (*T*) and zooplankton biomass (*P*) on the western Indian shelf between 8°N and 15°N. From Murty (1987).

An indication of a current reversal in the west is seen in September (Figure 11.4e). Currents are consistently southwestward and strong (0.5 m s^{-1} and more) north of 15°N, and close to the shelf southwestward flow prevails. Complete reversal of the East Indian Current into the *East Indian Winter Jet* is not achieved until late October, when water from the Equatorial Jet enters the Bay in the east and a cyclonic circulation is established. The East Indian Winter Jet is a powerful western boundary current with velocities consistently above 1.0 m s^{-1}. It follows the topography south of Sri Lanka and feeds its water into the Arabian Sea. Very little exchange occurs with the Equatorial Jet south of Sri Lanka; currents in the separation zone between the two jets (near 3°N) are weak and variable. The East Indian Winter Jet fades away from the north in late December, its southern part merging with the developing North Equatorial Current.

Western boundary currents

The story of the western boundary currents begins east of Madagascar, where both the integrated flow (Figure 4.7) and the ship drift currents show a separation of the South Equatorial Current into a northern and southern branch. The distribution of their transports - 30 Sv in the northern branch, 20 Sv in the southern branch - varies little over the year (Swallow *et al.*, 1988). The contribution of the northern branch to the circulation in the southern hemisphere is the Mozambique Current; it is maintained throughout the year. The contribution to the circulation in the northern hemisphere ceases during the Northeast Monsoon season. The southern branch feeds the *East Madagascar Current*. The current field of this small but well-defined western boundary current reaches to the 2000 m level. Below 3100 m some 4 - 5 Sv are carried northward, with little movement in-between. Having passed the southern tip of Madagascar the current apparently alternates between three flow

Entrainment of water from the loop increases the net southward flow to 15 Sv near 20°S. These estimates are based on a depth of no motion of 1000 m and do not include flow on the shelf, so they almost certainly underestimate the true transport of the Mozambique Current; but they leave little doubt that the East Madagascar Current is the more important source for the Agulhas Current.

The region south of Mozambique Strait is characterized by the frequent occurrence of cyclonic eddies (*d* in Figure 11.10), spawned by the passage of the joint flow from the Mozambique and East Madagascar Currents over the Mozambique Ridge. This ridge does not reach much higher than 1500 m; but the current reaches deep enough to be influenced by it. Figure 11.11 shows that the eddies are also deep-reaching energetic features, with life spans of many months and transports of 15 - 30 Sv.

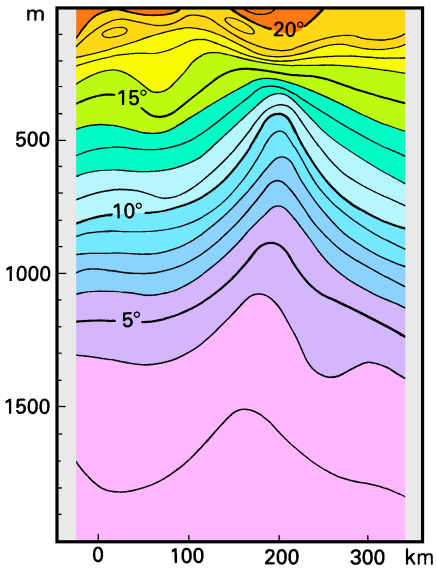

Fig. 11.11. A temperature section through a cyclonic eddy near the Mozambique Ridge. The form of the 3°C isotherm indicates that the eddy reaches deeper than 2000 m. See Fig. 11.10 for the location of the section. From Gründlingh (1985a).

South of 30°S the flow continues as the *Agulhas Current,* one of the strongest currents of the world ocean. In contrast to other western boundary currents it shows little seasonal variation. Mean speeds are 1.6 m s^{-1} throughout the year, and peak speeds exceed 2.5 m s^{-1} in most months. Transport estimates from observations give 70 Sv near 31°S and an increase of 6 Sv for every 100 km (as in the Gulf Stream). On approaching the shallow Agulhas Bank near 35°S it carries 95 - 135 Sv. The current occasionally floods the bank, lowering the inshore temperatures by several degrees (Figure 11.12). This upwelling is a result of the thermocline slope across the current (Rule 2 of Chapter 3) and not related to the wind. An increase in current speed increases the thermocline slope; since isotherm depths on the oceanic side of the current cannot change, the result is an uplift of cold water onto the shelf. Transport estimates for the Agulhas Current agree well with the depth-integrated estimate of Chapter 4 until the current rounds the Cape of Good Hope. Further south the current encounters the circumpolar eastward drift, and most of its transporr turns back into the Indian Ocean (Figure 11.13), quite in contrast to the

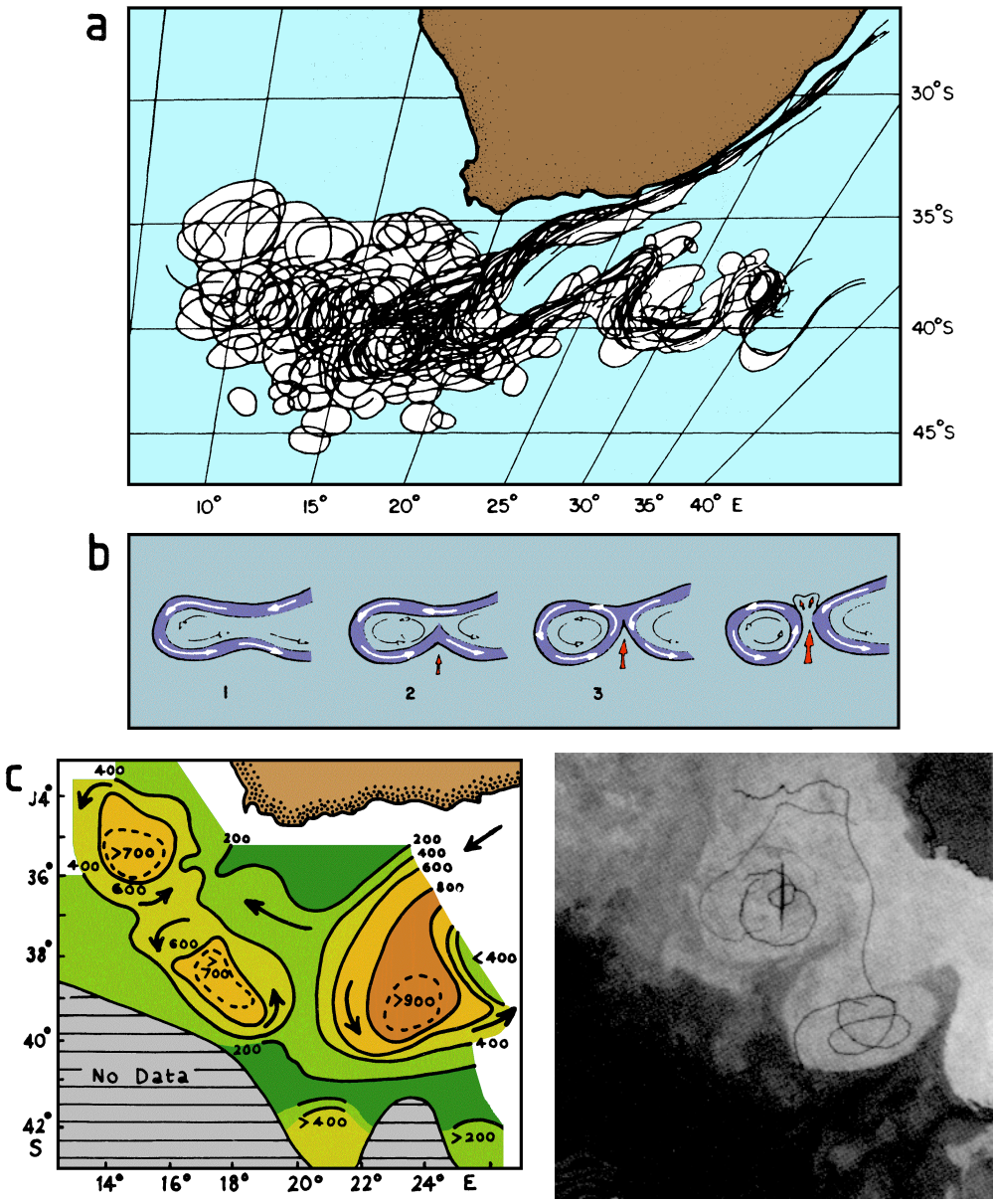

Fig. 11.13. The retroflection region of the Agulhas Current. (a) Positions of the temperature front along the Agulhas Current for a 12 month period 1984/85; (b) sketch of the eddy shedding process at the retroflection; (c) depth of the 10°C isotherm (representative for the thermocline) in November/December 1983; (d) sea surface temperature during 7 - 9 December 1983 and tracks of drifting buoys in November/December 1983. The area shown is approximately 32° - 42°S, 10° - 20°E. To minimize cloud disturbance the picture is a composite of three images. Lighter tones indicate warmer water. From Lutjeharms and van Ballegooyen (1988) and Gordon (1985).

surface temperature for May/June 1979. The dynamic structure of the upwelling region is identical to that of other coastal upwelling regimes (see for example the Peru/Chile upwelling in Chapter 8); the southward flow beneath 150 m mentioned above is in fact the continuation of its undercurrent. The increase in wind speed four weeks later strengthens the oceanic circulation, without destroying the two-gyre structure (Figure 11.17); current speeds can reach 3.5 m s^{-1} at the surface, and coastal temperatures in the two upwelling centres are lowered dramatically (Figure 11.16b). Reported transport estimates are 27 Sv above 100 m and 80 Sv between the surface and 700 m for the southern gyre, and 22 Sv above 100 m in the northern gyre. As the monsoon reaches its peak in August, the temperature front at 4°N is pushed northward along the coast until it merges with the Ras Hafun front; by September the Somali Current is established as a continuous western boundary current, from the Zanzibar Current in the south to the East Arabian Current in the north. The Ras Hafun gyre survives offshore as the "Great Whirl", keeping mixed layer depths greater than 200 m near 9 - 10°N, 53 - 54°E during the November transition and early Southwest Monsoon season when mixed layer depths are near 50 m elsewhere.

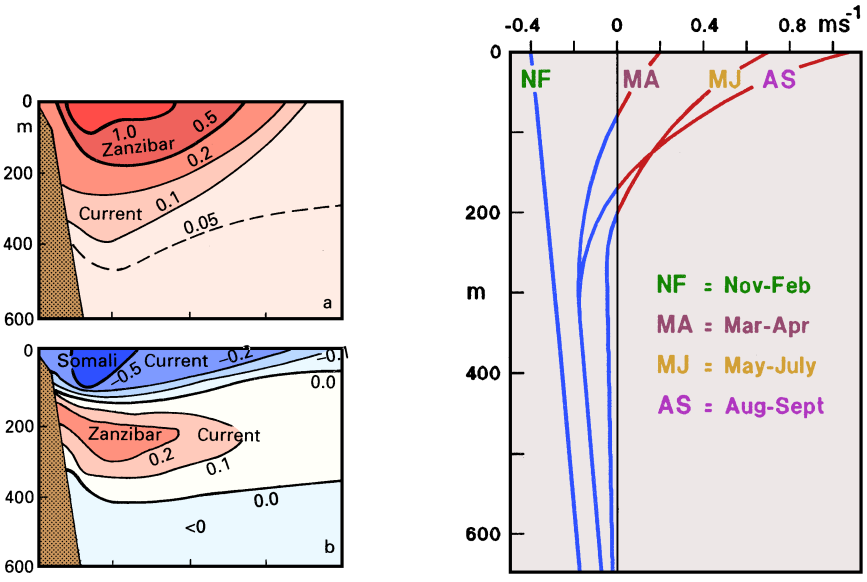

Fig. 11.14. (Left) Mean meridional current velocity (m s^{-1}) in the western boundary currents at the equator, derived from 2 years of observations during 1984 - 1986. (a) June - September, (b) December - February. After Schott *et al.* (1990).

Fig. 11.15. (Right) Mean alongshore velocity (positive = northeastward) in the Somali Current at 5°N, from 30 months of current meter records. After Quadfasel and Schott (1983).

generally does not generate marked surface cooling. Secondly, the monsoon wind reversal is so complete along this coast that the annual mean alongshore wind stresses here are close to zero, from the northern Bay of Bengal south to Java (Figure 1.4) and the upwelling in one season is counteracted by downwelling in the following season. Thirdly, twice a year (around May and November) the Equatorial Jet feeds warm water towards Sumatra, generating a pulse of current that flows poleward in both hemispheres. The seasonal cycle thus has strong semiannual as well as annual components, and is quite complicated. The strongest westward currents along the southern coast of Java, the seasonally reversing *South Java Current*, occur in August, when the monsoon winds are easterly and the Equatorial Jet is inactive. Surface cooling occurs off South Java at this time. This is also the time when the sea level difference from Java to Australia is largest, implying maximum strength in the Indonesian throughflow (see Chapter 13) and suggesting that at least some of the water for the South Java Current is then supplied from the Pacific Ocean.

The dynamics of the eastern boundary current along the western Australian coast, known as the *Leeuwin Current*, are very unusual and require some explanation. In the Pacific and Atlantic Oceans equatorward winds along the eastern boundary produce coastal upwelling, an equatorward surface flow, and a poleward undercurrent. In the Indian Ocean, annual mean winds along western Australia do blow towards the equator, but at the surface a vigorous poleward flow runs against the wind, and the undercurrent is equatorward. The reason is that eastern boundary currents are driven by the combined effects of alongshore winds and alongshore pressure gradients in the upper ocean. Figure 2.8b demonstrates that the upper ocean pressure distribution in the Indian Ocean differs substantially from those of the other oceans. While variations in dynamic height in the subtropics do not exceed 0.1 $m^2\ s^{-2}$ along most eastern coastlines, this difference is 0.5 $m^2\ s^{-2}$ (equivalent to about 0.5 m steric height) along western Australia. In the open ocean it drives an eastward geostrophic flow; but closer to the coast eastward flow becomes impossible, and the water accelerates down the pressure gradient. In the Indian Ocean the resulting poleward flow is strong enough to override the wind-driven equatorward current — and the onshore geostrophic flow is strong enough to override the offshore Ekman flow.

The large drop in steric height along western Australia is apparently related to the connection between the Pacific and Indian Oceans through the Australasian Mediterranean Sea. The free connection from the Pacific to the Indian Ocean permits steric height to have similar values at either end of the channel — i.e. the steric height off Northwest Australia is essentially the same as in the western equatorial Pacific Ocean (Figure 2.8b). Steric height is about 0.5 m larger than that off Peru, because the easterly winds blowing along the equatorial Pacific Ocean maintain the steric height gradient along the equator that can be seen in Figure 2.8b. The high steric height at 15°S off northwest Australia cannot be maintained at 34°S — steric height is primarily a depth-integral of temperature through eqn (2.3), and to maintain the same surface steric height at 34°S would require maintenance of an average temperature of about 25°C over the top 200m, in a region where strong winds and air temperatures of 12°C occur in winter. Strong cooling and convective overturn occurs (Figure 11.18), to bring water temperatures down nearer to air temperatures throughout a mixed layer typically 150m deep, near 34°S in winter. This heat loss can be seen in Figure 1.6, which shows that, unlike the other eastern boundaries, a net heat loss to the atmosphere occurs near the western Australian coast poleward of 20°S. It extends down to 150 m and results in relatively low steric height at the southern end of western Australia. The resulting southward flow in turn feeds the warm water pollards to maintain the surface

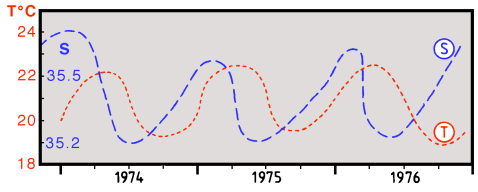

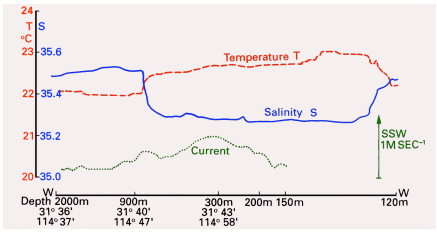

Fig. 11.19. (Left) Seasonal variation of surface temperature (*T*) and salinity (*S*) on the central shelf off Perth (32°S). Note the rapid drop of salinity between March and June; the Leeuwin Current is at its peak around April/May, bringing warm, fresh water from the tropics. From Cresswell and Golding (1980).

Fig. 11.20. (Right) A section across the Leeuwin Current off Perth (31°40'S), showing temperature and salinity fronts near 900 m and 120 m water depth on either side of the current. From Cresswell and Golding (1980).

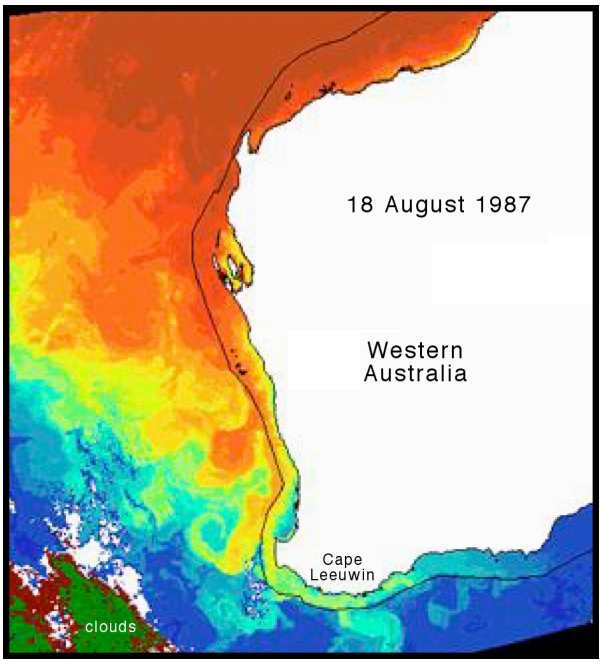

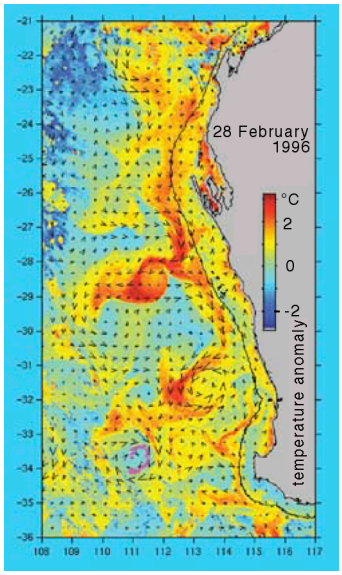

Fig. 11.21. Satellite images of sea surface temperature in the Leeuwin Current and associated eddies. Warm is red, cold is blue. Left: Sea surface temperature in August 1987. The Leeuwin Current is seen as a band of warm water along the western coastline that continues around Cape Leeuwin. The black line indicates the shelf break. (b) Sea surface temperature anomalies (departures from the latitudinal mean temperature) in February 1996 showing large eddies near Cape Leeuwin. Black arrows indicate surface currents. © CSIRO Marine Research, reproduced by permission.